Journal of Alloys and Compounds 513 (2012) 282–288

Contents lists available at SciVerse ScienceDirect

Journal of Alloys and Compounds

journal homepage: www.elsevier.com/locate/jallcom

Synthesis and properties of Co-doped $LiFePO_4$ as cathode material via a hydrothermal route for lithium-ion batteries

Rui-rui Zhao[a], I-Ming Hung[b], Yi-Ting Li[b], Hong-yu Chen[a,c,d,*], Chun-Peng Lin[b]

[a] School of Chemistry and Environment, South China Normal University, Guangzhou 510006, PR China
[b] Yuan Ze Fuel Cell Center/Department of Chemical Engineering and Materials Science, Yuan Ze University, No. 135, Yuan-Tung Road, Chungli, Taoyuan 320, Taiwan
[c] Base of Production, Education & Research on Energy Storage and Power Battery of Guangdong Higher Education Institutes, Guangzhou 510006, PR China
[d] Engineering Research Center of Materials and Technology for Electrochemical Energy Storage (Ministry of Education), South China Normal University, Guangzhou 510006, PR China

ARTICLE INFO

Article history:
Received 20 July 2011
Received in revised form 7 October 2011
Accepted 13 October 2011
Available online 20 October 2011

Keywords:
Coating materials
Electronic properties
Composite materials
Batteries
$LiFePO_4$

ABSTRACT

A series of olivine $LiFe_{1-x}Co_xPO_4$ composites were synthesised by a hydrothermal route under reductive atmosphere. The structure of the prepared samples was characterised by X-ray diffraction. Morphology, particle size, and elemental concentration were observed by scanning electron microscopy, high-resolution transmission electron microscopy, and corresponding EDS mapping, respectively. Raman spectroscopy was employed to study the surface information of the carbon-coated $LiFe_{1-x}Co_xPO_4$. The electrochemical properties of the samples were studied by AC impedance spectroscopy and charge–discharge instruments at room temperature. The discharge capacity of $LiFe_{3/4}Co_{1/4}PO_4$/C is 170 mAh/g at rate of 0.1 C. $LiFe_{1-x}Co_xPO_4$ can achieve a higher discharge plateau (~3.5 V) than does pure $LiFePO_4$ (~3.4 V). The results indicate that the Co-doped sample exhibits improved electrochemical performance at low discharge rates. However, XPS results show that the Li–O band stabilises further as the doping amount increase, which is not beneficial to the lithium diffusion coefficient of the compound.

1. Introduction

Lithium iron phosphate has attracted considerable interest as a positive electrode active material for Li-ion batteries because of its low cost, nontoxic properties, and safety, thereby presenting promising potential for use in hybrid electric vehicles [1,2]. However, its low electrical conductivity and low working voltage restricts its application in commercial products [3]. Carbon coating [4] and particle size reduction [5] are considered effective ways of improving the performance of lithium iron phosphate.

Aside from the aforementioned approaches, metal ion doping in the Li or Fe site is regarded as a promising method for increasing electrical conductivity and working voltage [6]. Cobalt [7,8], manganese [9], nickel [10], and vanadium [11] are considered favourable candidate dopants because of the higher chemical potential of $Co^{2+/3+}$, $Mn^{2+/3+}$, $Ni^{2+/3+}$, and $V^{2+/3+}$. To maximise the advantages of metal ion doping, multi-metal ion-doped compounds have also been prepared; these include $LiFe_{1/4}Mn_{1/3}Co_{1/3}PO_4$ [12] prepared via solid-state measurement and $LiFe_{1/4}Mn_{1/4}Co_{1/4}Ni_{1/4}PO_4$ [13] prepared by solid-state synthesis. To date, however, few systematic studies on cobalt doping have been conducted compared with those on other transition metals. A previous study [14] reported that a low cobalt doping amount does not increase the redox potential of $Fe^{2+/3+}$. Thus, increasing the discharge plateau necessitates high amounts of cobalt dopant.

Amongst various synthetic methods, such as solid-state reaction, co-precipitation method, and sol–gel route, hydrothermal reaction has been accorded substantial research efforts because this method enables facile carbon coating onto samples, and a small, homogeneous particle distribution in the end product [15,16]. It is relatively quick, simple, and requires mild operating temperatures. In addition, controlling the product properties by changing experimental parameters, such as temperature, pressure, and concentration, is convenient.

In this paper, a series of $LiFe_{1-x}Co_xPO_4$ composites were synthesised via hydrothermal reaction. Reductive atmosphere was employed in the heat treatment procedure to ensure the presence of Fe^{2+} and Co^{2+} in the end product. The structural characteristics and electrochemical performance of the composites were also investigated.

2. Experimental

2.1. Synthesis of $LiFe_{1-x}Co_xPO_4$/C

$LiFePO_4$ was prepared via a hydrothermal route using $LiOH{\cdot}H_2O$ (Alfa Aesar), $FeSO_4{\cdot}7H_2O$ (Sigma–Aldrich), H_3PO_4 (Sigma–Aldrich), and $(NH_4)_2HPO_4$ (J.T. Baker)

* Corresponding author at: School of Chemistry and Environment, South China Normal University, Guangzhou 510006, PR China. Tel.: +86 02039310183; fax: +86 02039310183.
E-mail addresses: hychen@scnu.edu.cn, battery_chy@126.com (H.-y. Chen).

0925-8388/$ – see front matter © 2011 Elsevier B.V. All rights reserved.
doi:10.1016/j.jallcom.2011.10.037

Table 1
Lattice parameters and unit cell volume for the samples.

Specimen	a (Å)	b (Å)	c (Å)	Volume (Å^3)
$LiFePO_4$	10.3203	5.9930	4.6720	288.96
$LiFe_{0.75}Co_{0.25}PO_4$	10.2997	5.9889	4.6878	288.39
$LiFe_{0.5}CO_{0.5}PO_4$	10.2898	5.9686	4.6957	287.14
$LiCoPO_4$	10.2005	5.9218	4.6984	283.81

as starting materials. $LiOH{\cdot}H_2O$ (Alfa Aesar) was first dissolved in purified water with continuous magnetic stirring. H_3PO_4 and $(NH_4)_2HPO_4$ were added into the solution after LiOH was completely melted and reacted for 10 min. $FeSO_4{\cdot}7H_2O$ and ascorbic acid were added subsequently. Another 30 min was needed to make the solution form a homogeneous solution, then the PH value was adjusted to 7 with $NH_3{\cdot}H_2O$ (Sigma–Aldrich) and H_3PO_4. To inhibit the conversion of Fe^{2+} to Fe^{3+} and Co^{2+} to Co^{3+}, water was degassed in a vacuum degasifier for 30 min prior to the preparation of the starting solution, after which the mixing process was carried out under an argon atmosphere. The molar ratio of the Li:Fe:P in the precursor solution was 3:1:1. In preparing the doping samples, $Co(NO_3)_2{\cdot}6H_2O$ was used as Co source.

About 110 mL starting solution was introduced into a Teflon reactor (inner volume: 200 mL), and then the reactor was sealed in a stainless steel autoclave and heated at 170 °C for 10 h. After being cooled to room temperature, the obtained precipitates were collected by centrifugation and washed several times with deionised water. The samples were then dried at 100 °C for 12 h in a vacuum oven. Finally, the samples were heat treated at 700 °C for 3 h under a 3%H_2/Ar reductive atmosphere.

2.2. Characterisation of synthesised materials

The crystallographic structure of the synthesised materials was analysed by X-ray powder diffraction (XRD; Shimadzu Labx XRD-6000) with Cu Kα (λ = 1.5406 Å) radiation. X-ray photoelectron spectroscopy (XPS; Thermo Fisfer-K-ALPHA) was used to obtain the valence state information of the samples with monochromatic Al Kα radiation ($h\nu$ = 1486.6 eV). The morphology and average particle size of the end products were observed using a JOEL JSM-6701F field emission scanning electron microscope. High-resolution transmission electron microscopy analysis was performed using a JEOL-2100 at a 200 kV acceleration voltage. Raman spectra were recorded on a laser Raman scattering spectrometer (Renishaw-Ramascope) to characterise the carbon properties coated onto the samples.

2.3. Electrochemical performance test

Electrochemical measurements were performed using a coin-type cell (model 2032). The cathode electrodes were fabricated by dispersing 80 wt% active material, 4 wt.% KS-4, 6 wt.% Super P, and 10 wt.% polyvinylidene fluoride in *N*-methyl pyrrolidone to form a slurry. The slurry was then coated onto an Al foil and the solvent was evaporated at 110 °C for 12 h under vacuum. The electrolyte was 1 M $LiPF_6$ in 1:1 ethylene carbonate and dimethyl carbonate. A lithium metal foil was used as the anode and a microporous polypropylene sheet (Celgard2320, Celgard Inc., USA) was used as the separator. The cell assembly was performed under an argon atmosphere in a glove box.

The charge–discharge and cycling properties of coin cells were evaluated between 2.5 and 5 V at 0.1*C* current density using an automatic galvanostatic charge–discharge unit (Neware) at room temperature. To test the real redox potential of the cation couples, GITT measurements were performed using a galvanostatic charge–discharge unit. A constant current at a rate of 0.1*C* was applied to the coin cell for 10 min, followed by a 40 min relaxation period. The measurement was continued until the cell voltage reached a fixed value. AC impedance was employed to characterise the composite cathode materials under open-circuit potential on a CHI614C instrument (CH Instrument Inc., USA). The frequency ranged from 10^{-2} to 10^5 Hz and the amplitude of overpotential was 0.005 V.

3. Results and discussion

3.1. Sample characterisation

Considering that the exchange of lithium ions with electrolyte occurs at the electrode–electrolyte interface, cathode performance critically depends on the electrode microstructure and morphology. The XRD patterns of the sample with different Co-doping amounts are shown in Fig. 1. All the samples are single phase except for $LiCoPO_4$ (JCPDS 85-0002), which contains Co_2P and Li_3PO_4 impurities. All the reflections can be indexed on the basis of the olivine structure with the space group *Pnma*. Table 1 shows the corresponding structural parameters and unit cell volume of the samples. The lattice parameters and unit cell volume slightly

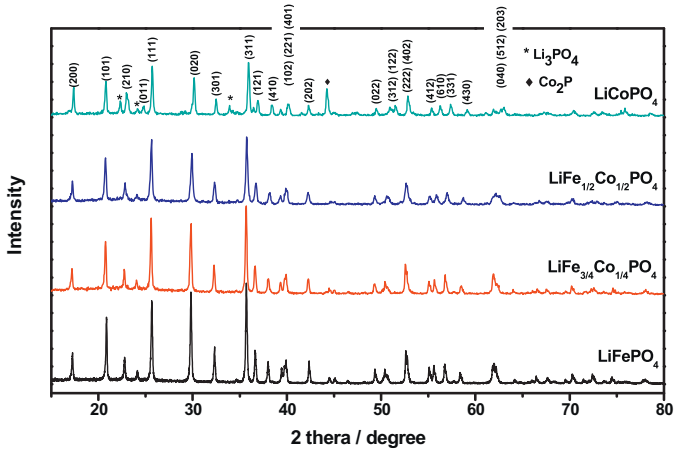

Fig. 1. XRD patterns of $LiFe_{1-x}Co_xPO_4$ samples.

decrease with increasing Co doping amount in the crystal. This result is attributed to the smaller ionic radii of Co^{2+} (0.75 Å) compared with that of Fe^{2+} (0.78 Å) [7].

Fig. 2 shows the morphologies of the $LiFe_{1-x}Co_xPO_4$ samples. The particle size of ellipsoid-shaped $LiFePO_4$ has a wide distribution range from 100 to 500 nm. However, $LiCoPO_4$ shows agglomeration because of the second phase of Li_3PO_4, which may have melted during the calcination process, thereby causing the agglomeration of $LiCoPO_4$ particles. However, the doped samples have smaller particle sizes and narrow particle size distribution, as well as a long ellipsoid shape. In particular, at a doping amount of 25% $LiFe_{3/4}Co_{1/4}PO_4$, the particle size is small and uniformly distributed, and no agglomeration occurs.

The particle shape can be observed more clearly by field emission scanning electron microscopy (FESEM). The results are shown in Fig. 3. The high-magnetisation images (insets) distinctly show that the carbon layer is coated onto the surface of the $LiFe_{1-x}Co_xPO_4$ particles. Furthermore, more carbon is coated onto the $LiFe_{1-x}Co_xPO_4$ particles with increasing cobalt doping amounts. The same conclusion can be obtained from the Raman analysis, the possible reason for which is discussed in the next section. Fig. 4(a) and (b) shows the elemental concentration images of the element mapping derived from the FESEM observations. These images clearly demonstrate that Fe, Co, P, and O are distributed homogeneously in the $LiFe_{1-x}Co_xPO_4$ particles. This result indicates that Co in the olivine structure of $LiFePO_4$ forms a $LiFe_{1-x}Co_xPO_4$ solid solution.

3.2. X-ray photoelectron spectroscopy

The oxidation states of Fe and Co were studied by XPS, and the results are shown in Fig. 5. The Fe 2p spectrum consists of two components because of spin-orbit coupling (Fe $2p_{3/2}$ and Fe $2p_{1/2}$) [17]. Each component consists of a main peak and a "shake-up" satellite. The binding energy position of the main peak is related to the oxidation state of Fe. For the Fe^{2+} ion in $LiFePO_4$, the main peaks of Fe $2p_{3/2}$ and Fe $2p_{1/2}$ are centred at 710.5 and 724 eV, respectively. For the Fe^{3+} ion in $FePO_4$, the main peaks of Fe $2p_{3/2}$ and Fe $2p_{1/2}$ are centred at 712.5 and 726 eV, respectively. The peak position in Fig. 5 is consistent with Fe^{2+}, and no peak assigned to Fe^{3+} appears in the samples. The Co 2p spectrum shape is similar to that of Fe 2p, and the core level matches well with Co^{2+} according to Co $2p_{3/2}$ and Co $2p_{1/2}$ observed at 780.9 and 796.7 eV, respectively. Thus, we can conclude that the oxidation states of Fe and Co are +2 in the synthesised samples.

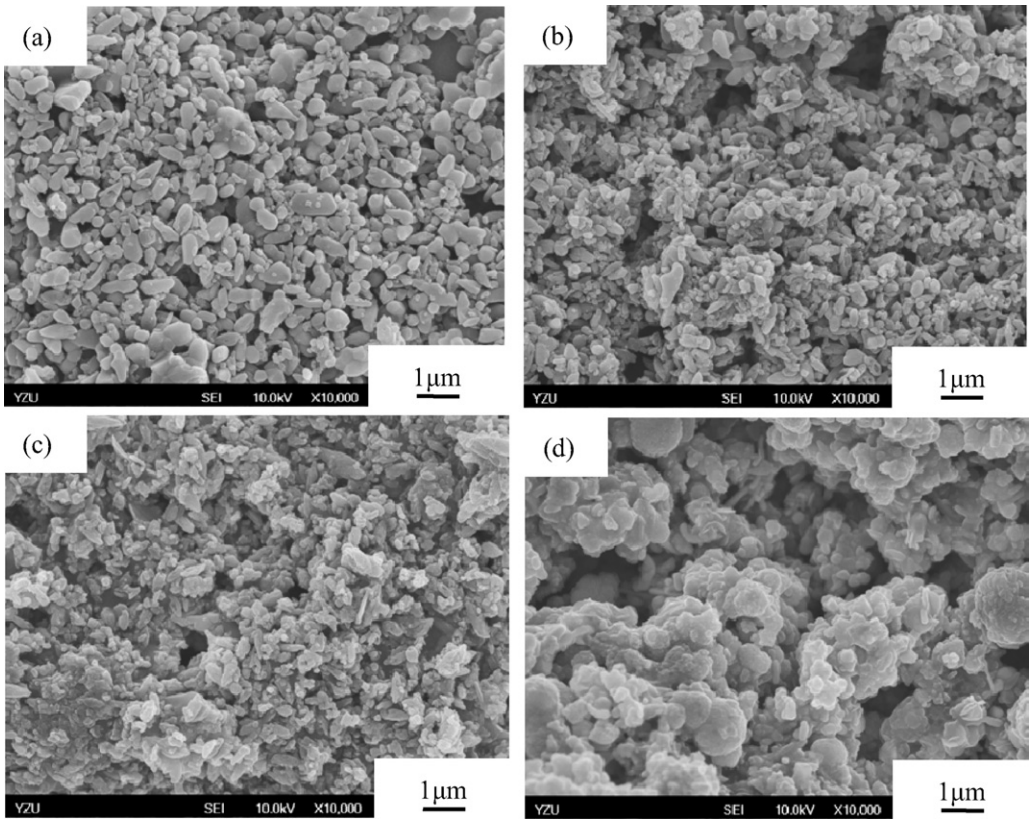

Fig. 2. SEM micrographs of carbon-containing $LiFe_{1-x}Co_xPO_4$ powders: (a) $x = 0$; (b) $x = 1/4$; (c) $x = 1/2$; (d) $x = 1$.

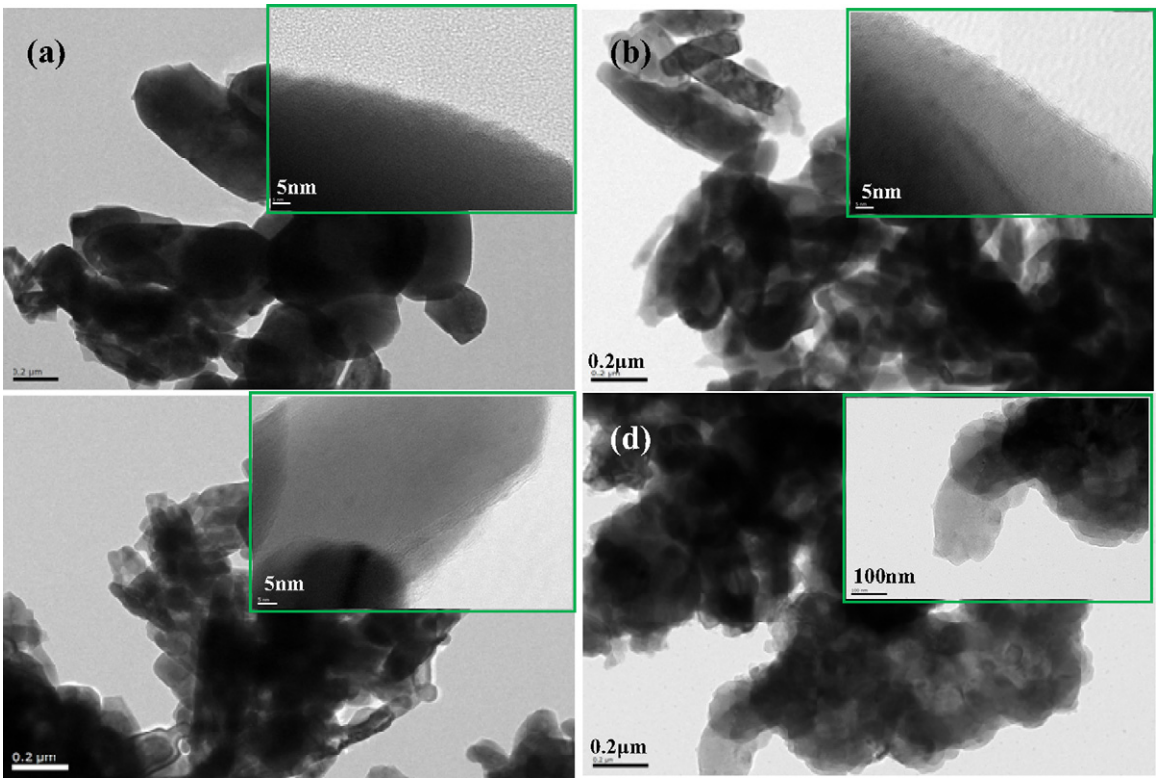

Fig. 3. TEM images of $LiFe_{1-x}Co_xPO_4$ with (a) $x = 0$; (b) $x = 1/4$; (c) $x = 1/2$; (d) $x = 1$.

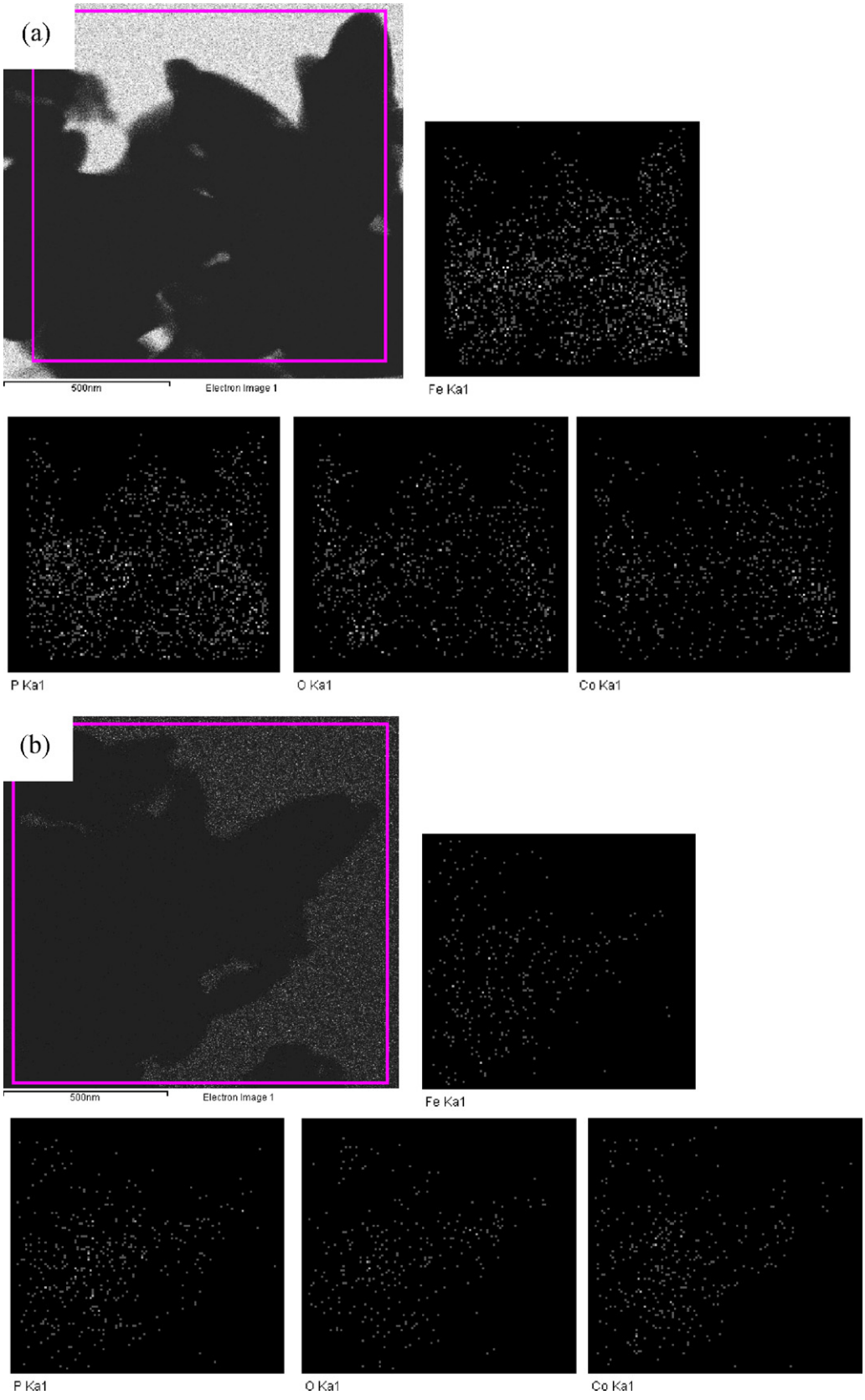

Fig. 4. EDS mapping of $LiFe_{1-x}Co_xPO_4$. (a) $x = 1/4$ and (b) $x = 3/4$.

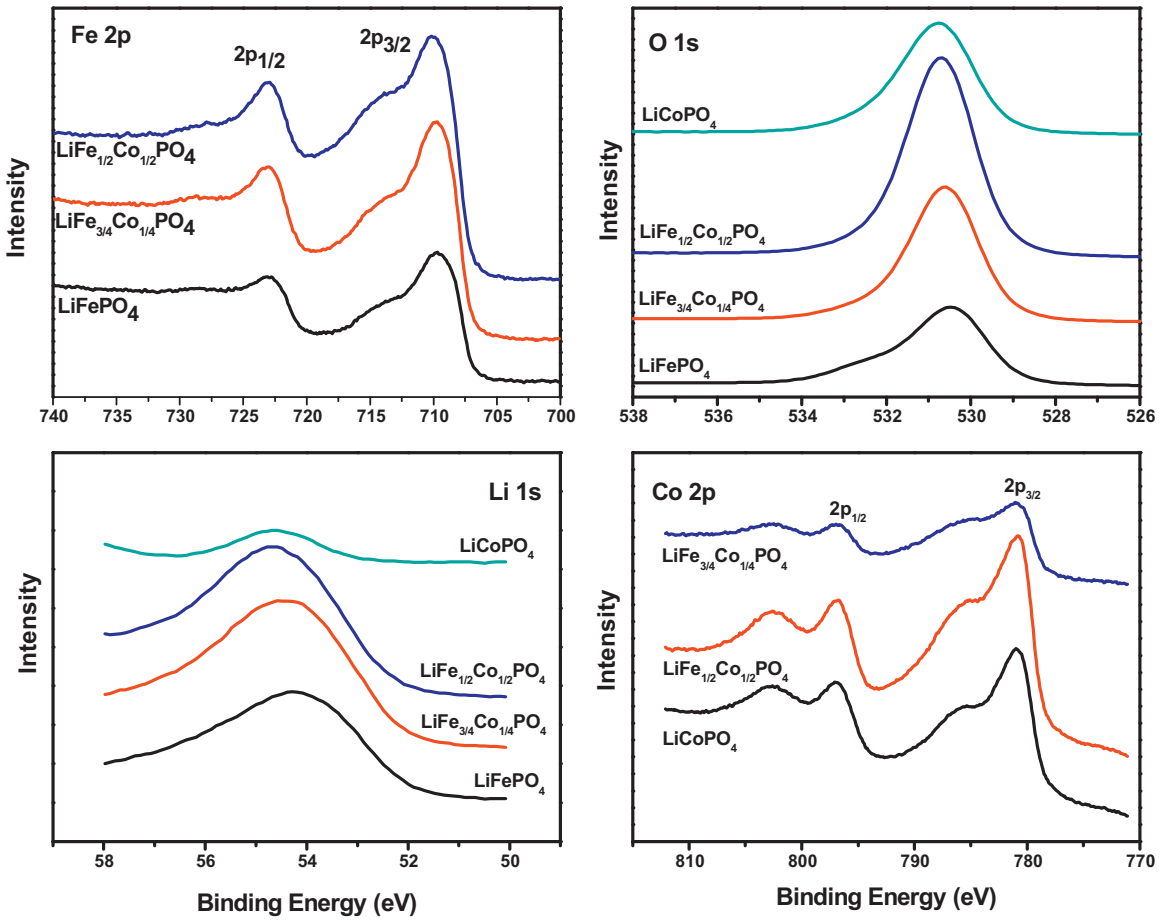

Fig. 5. XPS spectra of $LiFe_{1-x}Co_xPO_4$ samples.

The variations in the chemical environment of Li and O in $LiFe_{1-x}Co_xPO_4$ were also estimated by XPS [18]. Both the binding energy of O 1s and Li 1s slightly shift up as doping amount is periodically increased. This result is slightly different from that of a previous study [19]. The higher binding energy of an element may be ascribed to two factors: the enhancement of a bond and a high oxidation state of the element. The upward shift of the high binding energy indicates that more stable Li–O bands can be obtained because of Co doping, which may decrease the ionic mobility of Li^+ in the doped materials.

3.3. Electrochemical performance

Fig. 6 shows the discharge profiles of the $LiFe_{1-x}Co_xPO_4$/C solid solutions. Two obvious discharge plateaus correspond to the $Co^{2+/3+}$ and $Fe^{2+/3+}$ redox couples. The discharge plateau of pure $LiCoPO_4$/C is lower than its theoretical voltage possibly because of the existence of a large amount of impurities such as Li_3PO_4 and Co_2P. The discharge plateaus of $Co^{2+/3+}$ and $Fe^{2+/3+}$ clearly differ amongst the $LiFe_{1/2}Co_{1/2}PO_4$/C, $LiFe_{3/4}Co_{1/4}PO_4$/C, and $LiFePO_4$/C compounds. These results are consistent with the conclusions drawn by galvanostatic intermittent titration technique (GITT), discussed in the next section.

$LiFePO_4$/C delivers a discharge capacity of ~150 mAh/g with discharge rate of C/10, whereas that of $LiCoPO_4$/C is only 93 mAh/g. The doped samples exhibit good discharge capacity especially for $LiFe_{3/4}Co_{1/4}PO_4$/C, which delivers a capacity of ~170 mAh/g, a value that approximates the theoretical capacity of $LiFePO_4$. This result is attributed to the large contribution of $Fe^{2+/3+}$ to this compound and the smaller and fined particles.

Cell power is a crucial component of battery development. The power of the cells with the aforementioned materials was estimated using the integral areas of the discharge curves. Table 2 shows that the power of the cells in the cathode material of $LiFe_{3/4}Co_{1/4}PO_4$ and $LiFe_{1/2}Co_{1/2}PO_4$ are approximately 596 and 559 mW/g, respectively. These values are much higher than the

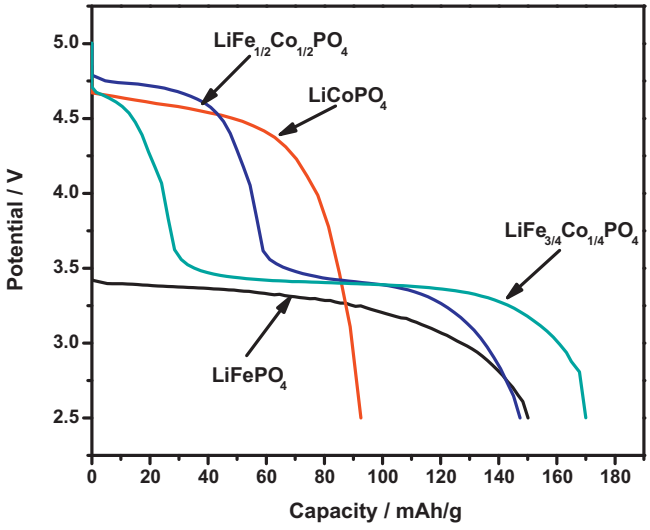

Fig. 6. First discharge curves of Li/C–$LiFe_{1-x}Co_xPO_4$ cells at a constant current of 0.1*C*.

Table 2
Integral areas of the discharge curves.

Material	Integral area (mW/g)
$LiFePO_4$	483
$LiFe_{3/4}Co_{1/4}PO_4$	596
$LiFe_{1/2}Co_{1/2}PO_4$	559
$LiCoPO_4$	400

power of the cells based on pure $LiFePO_4$ and $LiCoPO_4$ as cathode materials.

The GITT was first developed by Weppner and Huggins to determine the chemical diffusion coefficient of lithium in Li_3Sb [20]. In this paper, GITT was used to determine the true redox voltage of $Fe^{2+/3+}$ and $Co^{2+/3+}$. GITT measurements were carried out by applying a galvanic current at a rate of C/10 for 10 min, followed by a 40 min relaxation step. The current, relaxation, and so on were continued until the voltage reached a fixed potential. Fig. 7 shows the potential as a function of time based on the GITT measurement in the cell charging process. The redox potential of the $Fe^{2+/3+}$ couple increases in the Co-doped samples. The redox potential of the $Fe^{2+/3+}$ couple is 3.406 V for $LiFePO_4$, which increases to 3.448 and 3.469 V at Co doping amounts of 25% and 50%, respectively. According to Manthiram and Manthiram [7], the $Fe^{2+/3+}$ couple can be affected by the inductive effect introduced by the counter cations. In the present study, the $Fe^{2+/3+}$ redox potential increases because of the introduced $Co^{2+/3+}$.

These results indicate that the voltage of $LiFePO_4$ material can be improved and battery power can be enhanced by the introduction of Co.

3.4. Raman spectroscopy

Raman spectroscopy is a highly sensitive tool for studying the structure of lithium intercalation compounds; it has been widely used in Li-battery technology and the dynamics of lithium intercalation in different host materials [21].

The Raman spectra are shown in Fig. 8. Two intense bonds at around 1350 and 1590 cm^{-1} can be assigned to the characteristic Raman spectra of residual carbon in the samples. The bands at 1590 cm^{-1} mainly correspond to the graphitised structured carbon of the G bond, whilst the 1350 cm^{-1} band corresponds to the disordered structured carbon of the D bond. The signal observed at 945 cm^{-1} is related to the PO_4^{3-} anion symmetric stretching of

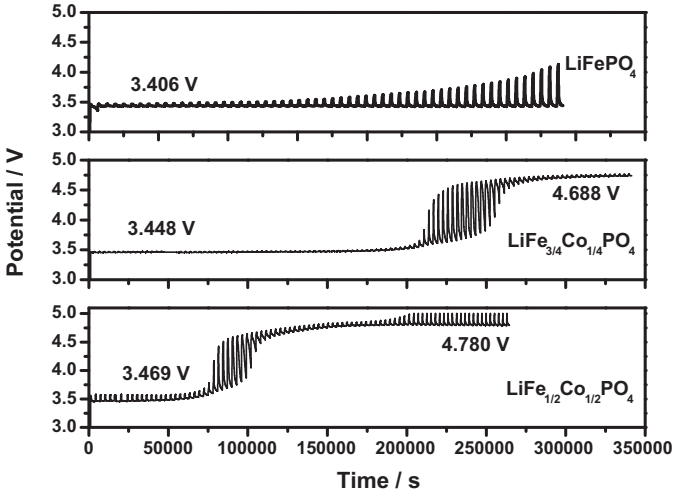

Fig. 7. Potential vs. time curves obtained for the $LiFe_{1-x}Co_xPO_4$ samples from GITT measurement.

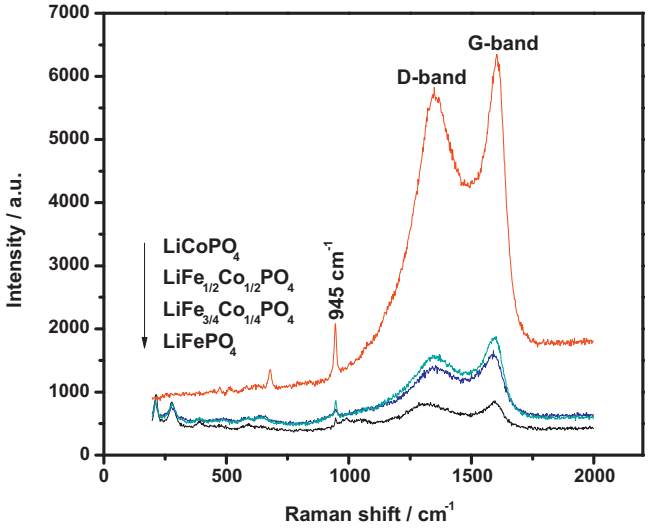

Fig. 8. Raman spectral curves of olivine $LiFe_{1-x}Co_xPO_4$.

$LiFePO_4$. This signal is the strongest peak of this anion in the olivine spectrum.

The relative intensity ratio, $R = I_D/I_G$, defines the level of order and in-plane crystal size for pyrolytic carbon [22]. A low I_D/I_G ratio indicates the presence of a larger amount of graphene or sp^2-coordinated carbon compared with the disordered carbon structure (sp^3-coordinated carbon), which can improve the electrical conductivity of $LiFePO_4$ powders. The electrochemical properties of cathode materials strongly depend on the I_D/I_G ratio because more carbon of the G bond increases electrode conductivity [23,24]. The I_D/I_G values of the samples are shown in Table 3. The amount of G bond carbon in Co-doped $LiFePO_4$ powders is higher than that in $LiFePO_4$ and $LiCoPO_4$. $LiFe_{1/4}Co_{3/4}PO_4$ and $LiFe_{1/2}CO_{1/2}PO_4$ are expected to have higher conductivity.

Although Raman intensity is usually insignificant in material analysis, the intensity rises with increased Co doping amount (Fig. 8). This result is related to two factors: carbon content and $LiFe_{1-x}Co_xPO_4$/C composite bonds. Including a carbon source in the experiment serves two purposes: one is to increase the electrical conductivity of the material, and the other is to prevent the oxidation of Fe^{2+} and Co^{2+}. Because Co^{2+} is not as prone to oxidation as Fe^{2+}, more residual carbon is found in the bulk material, thereby resulting in higher carbon intensity in the Raman measurement. This result is in accordance with the TEM results. The increased Raman intensity is also related to the bonds in the $LiFe_{1-x}Co_xPO_4$/C composite, an issue that requires further research to confirm.

3.5. Electrochemical impedance spectroscopy experiment

Fig. 9 shows the Nyquist plots of the impendence spectra of the $LiFe_{1-x}Co_xPO_4$ compounds at open circuit conditions. The spectra typically consist of a semi-circle in the high frequency region and an inclined line at low frequency. The semi-circle is related to the electrode/electrolyte interface resistance, and the inclined line is attributed to the Warburg impedance associated with lithium ion

Table 3
Calculated I_D/I_G values of the samples.

Sample	I_D/I_G
$LiFePO_4$	0.975
$LiFe_{3/4}Co_{1/4}PO_4$	0.845
$LiFe_{1/2}Co_{1/2}PO_4$	0.868
$LiCoPO_4$	0.902

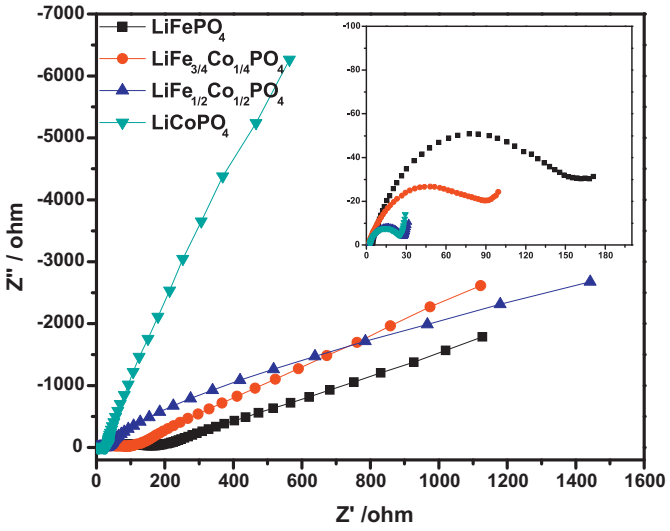

Fig. 9. Nyquist plots of $LiFe_{1-x}Co_xPO_4$ obtained at open circuit potential.

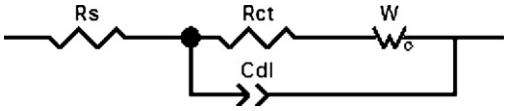

Fig. 10. Equivalent circuits used to fit the impedance spectra.

Table 4
Impedance parameters of $LiFe_{1-x}Co_xPO_4$ based on the equivalent circuit of Fig. 10.

Sample	R_s (ohm)	R_{ct}	C_{dl}	W_c
$LiFePO_4$	4.2	127.6	0.79	125.9
$LiFe_{3/4}Co_{1/4}PO_4$	1.6	74.5	0.72	75.4
$LiFe_{1/2}Co_{1/2}PO_4$	2.2	25.2	0.74	5.4
$LiCoPO_4$	2.7	20.3	0.79	16.74

diffusion in the electrode. An equivalent circuit (Fig. 10) is used to fit the impedance spectra. The fitted impedance parameters are shown in Table 4. R_s and R_{ct} represent the solution resistance and charge transfer resistance, respectively, and w is a coefficient pertaining to mass transfer.

The size of the semi-circle and the corresponding fitted R_{ct} value rapidly decrease, indicating a significant decrease in interface resistance and increase in electrical conductivity. The increased conductivity is due primarily to the enhanced electrical conductivity because of the presence of pyrolytic carbon webs, which stem from the higher residual carbon that resulted from the increased Co doping amount. These observations were confirmed by TEM and Raman analysis.

4. Conclusion

$LiFe_{1-x}Co_xPO_4$/C cathode materials were synthesised by hydrothermal method under a reductive atmosphere. The samples exhibit an olivine structure. The morphologies of the Co-doped samples are smaller and more uniformly distributed long ellipsoid particles compared with that of inhomogeneous pristine $LiFePO_4$. All the Co-doped samples exhibit two discharge plateaus in the discharge profile. $LiFe_{3/4}Co_{1/4}PO_4$ samples show a superior discharge capacity of 170 mAh/g at 0.1C, which is nearly equal to the theoretical capacity of $LiFePO_4$.

Co doping with large amount can increase the voltage of the $Fe^{2+/3+}$ oxide couple, and reduce the redox potential of $Co^{2+/3+}$. Moreover, the power of the Co-doped samples is higher than that of $LiFePO_4$ and $LiCoPO_4$. This result is highly significant in the development of lithium-ion cathode materials for high-voltage applications.

The amount of carbon coated onto the compound increases as Co doping amount rises. This result is due to more residual carbon in the compound, which is beneficial to the improvement of the electrical conductivity of the composite materials. However, the XPS results show that lithium diffusion coefficient cannot be effectively improved by Co^{2+}-doping because the Li–O band stabilises further.

Acknowledgment

The authors acknowledge the financial support from Taiwan under contract No. NSC99-2632-E-155-001-My3.

References

[1] L.X. Yuan, Z.H. Wang, W.H. Zhang, Energy Environ. Sci. 4 (2011) 269–284.
[2] S. Ferrari, R.L. Lavall, D. Capsoni, J. Phys. Chem. C 114 (2010) 12598–12603.
[3] Y.S. Hu, Y.G. Guo, R. Dominko, M. Gaberscek, J. Jamnik, J. Maier, Adv. Mater. 19 (2007) 1963–1966.
[4] R. Yang, X.P. Song, M.S. Zhao, F. Wang, J. Alloy Compd. 468 (2009) 365–369.
[5] J.F. Ni, M. Morishita, Y. Kawabe, M. Watada, N. Takeichi, T. Sakai, J. Power Sources 195 (2010) 2877–2882.
[6] G. Kobayashi, A. Yamada, S.I. Nishimura, R. Kanno, Y. Kobayashi, S. Seki, Y. Ohno, H. Miyashiro, J. Power Sources 189 (2009) 397–401.
[7] T. Muraliganth, A. Manthiram, J. Phys. Chem. C 114 (2010) 15530–15540.
[8] N. Penazzi, M. Arrabito, M. Piana, J. Eur. Ceram. Soc. 24 (2004) 1381–1384.
[9] C.F. Li, N. Hua, C.Y. Wang, X.Y. Kang, T.D. Wumair, Y. Han, J. Alloys Compd. 509 (2011) 1897–1900.
[10] Y.C. Ge, X.D. Yan, J. Liu, Z.F. Zhang, J.W. Wang, X.G. He, R.S. Wang, H.M. Xie, Electrochim. Acta 55 (2010) 5886–5890.
[11] M.R. Roberts, G. Vitins, J.R. Owen, J. Power Sources 179 (2008) 754–762.
[12] Y.C. Chen, J.M. Chen, C.H. Hsu, J.J. Lee, T.C. Lin, J.W. Yeh, H. Shih, J. Power Sources 195 (2010) 6867–6872.
[13] X.J. Wang, X.Q. Yu, H. Li, X.Q. Yang, J. Mcbreen, X.J. Huang, Electrochem. Commun. 10 (2008) 1347–1350.
[14] D. Shanmukaraj, G.X. Wang, R. Murugan, Mater. Sci. Eng. C 149 (2008) 93–98.
[15] J.L. liu, R.R. Jiang, X.Y. Wang, T. Huang, A. Yu, J. Power Sources 194 (2009) 536–540.
[16] N. Recham, L. Dupont, M. Courty, Chem. Mater. 21 (2009) 1096–1107.
[17] R. Dedryvère, M. Maccario, L. Croguennec, Chem. Mater. 20 (2008) 7164–7170.
[18] D.Y. Wang, H. Li, S.Q. Shi, X.J. Huang, L.Q. Chen, Electrochim. Acta 50 (2005) 2955–2958.
[19] D.Y. Wang, Z.X. Wang, X.L. Huang, L.Q. Chen, J. Power Sources 146 (2005) 580–583.
[20] W. Weppner, R.A. Huggins, J. Electrochem. Soc. 124 (1977) 1569–1578.
[21] E. Markevich, R. Sharabi, O. Haik, V. Borgel, G. Salitra, D. Aurbach, G. Semrau, M.A. Schmidt, N. Schall, C. Stinner, J. Power Sources 196 (2011) 6433–6439.
[22] C.Z. Lu, G.T. Fey, H.M. Kao, J. Power Sources 189 (2009) 155–162.
[23] M.M. Doeff, J.D. Wilcox, R. Kostecki, G. Lau, J. Power Sources 163 (2006) 180–184.
[24] J.K. Kim, J.W. Choi, G.S. Chauhan, J.H. Ahn, G.C. Hwang, J.B. Choi, H.J. Ahn, Electrochim. Acta 53 (2008) 8258–8264.